Journal of Inflammation Research

Dovepress
Taylor & Francis Group

Open Access Full Text Article

ORIGINAL RESEARCH

DNA-PKcs Dysfunction Enhances the Antitumor Activity of Radioimmunotherapy by Activating the cGAS-STING Pathway in HNSCC

Lizhu Chen[1–3,*], Jing Lin[1–3,*], Yaoming Wen[4,*], Zeng-Qing Guo[1–3,*], Bin Lan[2,3], Jiani Xiong[1–3], Chuan-Ben Chen[2,3,5], Yu Chen[1–3]

[1]Department of Medical Oncology, Clinical Oncology School of Fujian Medical University, Fujian Cancer Hospital, Fuzhou, Fujian Province, People's Republic of China; [2]Cancer Bio-Immunotherapy Center, Clinical Oncology School of Fujian Medical University & Fujian Cancer Hospital, Fuzhou, Fujian Province, People's Republic of China; [3]Fujian Provincial Key Laboratory of Translational Cancer Medicine, Clinical Oncology School of Fujian Medical University & Fujian Cancer Hospital, Fuzhou, Fujian Province, People's Republic of China; [4]Department of Drug Research and Development, Fujian Institute of microbiology, Fuzhou, Fujian Province, People's Republic of China; [5]Department of Radiation Oncology, Clinical Oncology School of Fujian Medical University, Fujian Cancer Hospital, Fuzhou, Fujian Province, People's Republic of China

*These authors contributed equally to this work

Correspondence: Yu Chen; Chuan-Ben Chen, Email chenyu1980@fjmu.edu; ccb@fjmu.edu.cn

Introduction: Combining radiotherapy (RT) with immunotherapy for head and neck squamous cell carcinoma (HNSCC) has limited effectiveness due to the DNA damage repair (DDR) pathway activated by ionizing radiation. DNA-PK, encoded by the *PRKDC* gene, plays a key role in this repair. The potential improvement of radioimmunotherapy by inhibiting the DDR pathway is still unclear.

Methods: The effectiveness of different treatments on tumor growth and survival was tested using the C3H/HeN mouse tumor model. Flow cytometry analyzed treatment-induced immunophenotypic changes. In vitro, Western blot and PCR confirmed the impact of combining immunotherapy with RT on the cGAS-STING pathway after DNA-PKcs dysfunction.

Results: The combination of a DNA-PK inhibitor (NU7441), radiation therapy, and a PD-1 checkpoint inhibitor showed improved antitumor effects and extended survival in mice. Adding NU7441 into the RT and immunotherapy regimen increased CD8+ T cell infiltration. *PRKDC* alterations or DNA-PKcs dysfunction increased IR-induced DNA breaks, activating the cGAS-STING pathway and boosting the anti-tumor immune response.

Conclusion: These findings suggest that targeting the DDR pathway may represent a promising therapeutic strategy and biomarker to improve the efficacy of radioimmunotherapy in HNSCC.

Keywords: head and neck squamous cell carcinoma, *PRKDC*, cGAS-STING, radioimmunotherapy, DNA-PK

Introduction

Head and neck squamous cell carcinoma (HNSCC) is a prevalent cancer worldwide. In the US, approximately 55,000 new cases and 12,000 deaths from HNSCC are expected by 2023.[1] HNSCC responds well to radiotherapy (RT), making it an effective treatment for early-stage cases by preserving organ function and improving long-term survival rates.[2] However, over 60% of patients with HNSCC are diagnosed at advanced or locally advanced stages.[3] Despite aggressive treatment, these patients face a high risk of local recurrence and potential metastasis.[4] Immune checkpoint inhibitors (ICIs) such as Nivolumab and Pembrolizumab have shown promise in treating patients with HNSCC having a specific combined positive score (CPS) >20 of Programmed cell death 1 ligand 1 (PD-L1).[5,6] Nevertheless, the clinical response rate of Nivolumab and Pembrolizumab as standalone treatments in Asian patients is reported to be merely 20% based on available data.[7] Thus, this study aims to identify alternative biological markers beyond PD-L1 to expand the population responsive to immunotherapy and enhance the effectiveness of PD-1 inhibitors through various combination strategies.

Received: 23 September 2024
Accepted: 11 March 2025
Published: 19 March 2025

RT is frequently used to treat HNSCC and has demonstrated potential in enhancing the effectiveness of ICIs by altering the tumor immune microenvironment,[8] and may even induce an "abscopal effect".[9] The combination of RT and ICIs has been extensively studied in HNSCC,[10,11] with positive tumor responses reported in clinical case studies.[10,11] However, not all RT can sensitize ICIs, and the clinical occurrence of the "abscopal effect" remains low, with a maximum incidence of 10%.[12] A Phase II clinical study by McBride et al confirmed the safety of using single lesion RT with Nivolumab,[13] but no significant clinical benefit was observed. The NCT02952586 study,[14] a Phase III trial on concurrent chemoradiotherapy and immunotherapy for HNSCC, was terminated due to a lack of clinical benefit in the interim analysis. This suggests that the immune activation mechanism of radiation therapy for tumors is complex, involving various factors within the tumor microenvironment and the tumor itself.

Ionizing radiation (IR) can cause DNA double-strand breaks (DSBs) and activate the DNA damage repair (DDR) pathway. Inhibiting specific proteins involved in DNA repair can increase PD-L1 expression, thereby suppressing the immune microenvironment.[15] Consequently, modulating the DDR pathway through RT may influence the effectiveness of both RT and ICIs.

PRKDC encodes the protein DNA-dependent protein kinase catalytic subunit (DNA-PKcs), a crucial kinase responding to DNA damage. DNA-PKcs is integral to the non-homologous end joining (NHEJ) of DSBs and maintaining chromosome stability.[16] Phosphorylation of DNA-PKcs by IR aids in repairing DNA damage in tumor cells.[17] Conversely, DNA-PKcs inhibitors impede DNA damage repair. Mice treated with the DNA-PKcs inhibitor NU7441 in the RT group exhibited lower survival rates, demonstrating strong evidence of radiosensitization.[18] NU7441 has been shown to prolong IR-induced DSB duration and cause G2/M cell cycle accumulation.[19] Additionally, NU7441 enhances γH2AX foci formation, suppressing Mitoxantrone-induced DNA-PKcs autophosphorylation and repair.[20] Furthermore, NU7441 can decrease the frequency of NHEJ.[21] DNA-PK deficiency enhances cGAS-mediated antiviral innate immunity.[22] Previous studies indicated that using the DNA-PK inhibitor Peposertib with radiation increases susceptibility to anti-PD-L1.[23] The DDR inhibitor AZD6738 has also been investigated in combination with RT and ICIs in hepatocellular carcinoma.[24] Our previous findings suggest that *PRKDC* mutation plays a crucial role in increasing tumor mutational burden (TMB), promoting an inflamed tumor microenvironment (TME), and enhancing the response to ICIs.[25] Thus, *PRKDC* mutation can serve as a reliable predictor of favorable clinical outcomes associated with ICI treatment.

Combining RT with immunotherapy has shown limited effects in HNSCC. Initially, we identified the potential of NU7441 to enhance radioimmunotherapy. Consequently, this study aims to investigate how *PRKDC* alteration or DNA-PK dysfunction affects the tumor immune microenvironment and the outcomes of radioimmunotherapy. Our findings indicate that this enhancement is achieved by activating the cGAS-STING pathway and increasing CD8+ T cell infiltration in the TME.

Materials and Methods

Chemicals

NU7441, obtained from SELLECK (S2638, KU-57788), was administered to cells to achieve a final DMSO concentration of 1.0μM. In vivo experiments were conducted following rigorous review and approval by institutional animal welfare committees, in compliance with national regulations.

Cell Culture

CAL27 and FADU cells were procured from the American Type Culture Collection (ATCC), while SCC7 cells were generously provided by Professor Li Qing. All cells were cultivated in DMEM (Dulbecco's Modified Eagle Medium) supplemented with 10% FBS (fetal bovine serum). Following an 8-hour treatment with NU7441, cells underwent radiation therapy.

Antibodies

Alexa Fluor 647 anti-mouse CD4 (GK1.5) and APC750 anti-mouse CD8a (53–6.7) were obtained from Abcam. The following antibodies were acquired from Cell Signaling Technology: cGAS (D3080) Rabbit mAb (catalog 31659S), TBK1/NAK (D1B4) Rabbit mAb (catalog 3504S), IRF-3 (D83B9) Rabbit mAb (catalog 4302S), STING (D1V5L) Rabbit mAb (catalog 50494S), Phospho-IRF-3 (Ser396) (D601M) Rabbit mAb (catalog 29047S), Phospho-TBK1/NAK (Ser172)

(D52C2) Rabbit mAb (catalog 5483S), and Anti-rabbit IgG, HRP-linked Antibody (catalog 7074V). Servicebio supplied Anti-CD4 Rabbit pAb (catalog GB11064), Anti-CD8 alpha Rabbit pAb (catalog GB114196), Anti-FOXP3 Rabbit pAb (catalog GB11093), Anti-Ki67 Rabbit pAb (catalog GB111141), and Anti-PD-L1 Rabbit pAb (catalog GB11339A). GAPDH (14C10) Rabbit mAb (catalog 2118S) was also sourced from Cell Signaling Technology. Phospho-Histone H2A.X (Ser139) Antibody (catalog 2577) and Anti-dsDNA (clone AC-30-10, CBL 186) were purchased from MilliporeSigma. DNA-PK Recombinant Rabbit Monoclonal Antibody (SC57-08) (catalog A5-32192) was procured from Thermo Fisher Invitrogen.

Cell Culture and Transfection

FADU cells were cultivated in DMEM. The GV493 RNA interference (RNAi) system (Shanghai GeneChem Co., Ltd.) was used to generate lentiviruses expressing short interfering RNA sequences targeting *PRKDC* (LV-*PRKDC*-RNAi).[26,27] This system contains a U6 promoter-driven multiple cloning site (MCS) and a cytomegalovirus promoter-driven puromycin gene. The target sequence of *PRKDC* was 5'-TTTGTGCCGTCAACTTGTATG-3'. The vector used for *PRKDC* shRNA was GV493:hU6-MCS-CBh-gcGFP-IRES-puromycin. Lentiviral vectors interfering *PRKDC* (LV-*PRKDC*) were purchased from Shanghai GeneChem Co., Ltd. directly and were generated using the GV493 system (Shanghai GeneChem Co., Ltd). Briefly, the expression of shRNA, which is inserted into MCS, is driven by the U6 promoter, and the expression of green fluorescent protein (GFP) and puromycin expression, which are separated by internal ribosome entry site (IRES), is driven by the CBh promoter. The negative control lentiviruses, LV-NC-RNAi and LV-NC, were also purchased from Shanghai GeneChem Co., Ltd. The scrambled sequence used for the LV-NC-RNAi was as follows: 5'-TTCTCCGAACGTGTCACGT-3'. An empty lentiviral vector was used to transfect cells in the LV-NC group.

PRKDC-targeting shRNA minigenes were then used to infect CAL27 and FADU cells. Prior to transfection, cells were seeded in six-well plates at a density of 1×10^5 cells/well in complete medium and incubated overnight. Lentiviruses (multiplicity of infection=10) together with 5 μg/mL polybrene, was then added to the cells. At 24 h following infection, the culture medium was replaced with fresh medium containing 2 μg/mL puromycin (Sangon Biotech Co., Ltd., Shanghai, China), followed by positive selection for 3 days. The cells were then maintained in complete medium containing 1 μg/mL puromycin.

Establishment of Subcutaneous HNSCC Models

Male C3H/heN mice (5–7 weeks) were obtained from Beijing Vital River Laboratory Animal Technology Co., Ltd. The ethical and legal approval for the animal experiment was obtained from Fujian Cancer Hospital Ethics committee prior to the commencement of the study. All experiments were performed in accordance with relevant named guidelines and regulations. The authors complied with the ARRIVE guidelines. Subcutaneous implantation of SCC7 cells (3×10^5) was performed in the submandibular regions of these mice. Tumor volumes were calculated using the formula: length × $\text{width}^2/2$. Radiation therapy was administered when tumors reached approximately 100 mm^3. Tumor volume was subsequently measured every 3 days. In accordance with ethical guidelines, mice were euthanized upon reaching a tumor volume of 1500 mm^3. The 36th day following SCC7 cell implantation was designated as the endpoint.

Mouse Treatments

Mice were exposed to three fractions of 2 Gy radiation on days 1, 3, and 5 following the commencement of treatment. NU7441 (10 mg/kg) was administered intraperitoneally on the same days. In the PD-1 blockade experiment, anti-PD-1 (BioXcell, clone: 29F.1A12, Catalog #: BE0273, 2 mg/kg) was administered intraperitoneally on days 1, 4, and 7. On day 8 after treatment initiation, the mice were anesthetized by intraperitoneal injection with 2% sodium pentobarbital solution and sacrificed by cervical dislocation. Tumor tissues were extracted for subsequent analysis.

Analysis of TILs by Flow Cytometry

EGFP-expressing cells were quantitatively determined using an FACS Aria III cell sorter or BD FAC Symphony TM system (Becton Dickinson). Before analysis, samples were suspended in PBS and filtered through a 70 μm nylon mesh filter. FL1 (green fluorescence) readings were obtained using voltage and gain settings of 300 and 1.00 in log mode. For surface staining, samples were incubated with antibodies in the staining buffer for 30 minutes at 4°C. The antibodies used were CD4-PerCP-Cy5.5 and CD8a-APC (BD Biosciences). A total of 10,000 cells per sample were analyzed. To assess EGFP expression in PBMC, cells

transfected for 24 hours were selected based on FSC/SSC parameters to identify the lymphocyte population, followed by live cell identification using FVS-BV450 and GFP gating to evaluate the transfected cell population. For the analysis of EGFP expression in resting T cells, cells were sequentially gated for CD4+CD8a+GFP+. The BD FAC Symphony TM system was used for all cell acquisition, with data acquisition and analysis performed using FlowJo software (Becton Dickinson).

Western Blot Analysis

After treatments, cells were collected in a lysis buffer with protease and phosphatase inhibitors (Thermo Fisher, CA, USA). The cell lysates were centrifuged, and the resulting supernatants were collected. Total protein concentrations were measured using a BCA protein assay kit (Thermo Fisher, CA, USA). Equal amounts of proteins were separated by SDS-PAGE and transferred onto a Thermo Fisher PVDF membrane. The membrane was incubated with the primary antibody, followed by incubation with a goat anti-mouse IgG secondary antibody. Reactive bands were visualized using the Odyssey CLx Imaging System (LI-COR Biosciences, USA). GAPDH was used as a loading control. Protein expression levels were quantified using NIH ImageJ software.

RNA Isolation and Real-Time PCR

RNA was extracted from cells using Trizol reagent (Thermo Fisher, CA, USA.) cDNA synthesis was performed using the PrimeScript™ II 1st Strand cDNA Synthesis Kit (Takara, Shiga, Japan). Quantitative real-time PCR (qPCR) was conducted using SYBR® Premix Ex Taq™ Mix (Takara, Shiga, Japan) and the QuantStudio™ 6 Real-Time PCR Instrument (Thermo Fisher, CA, USA). Expression levels were normalized to β-actin, and relative expression changes were calculated using the $2^{-\Delta\Delta Ct}$ method. The qPCR analysis utilized the primers listed in Table 1:

RNA-Seq Analysis

Total RNA was isolated from samples, and cDNA library construction and sequencing were performed by BGI Genomics (BGI-Shenzhen, China) using the BGISEQ-500 platform. Gene expression levels were normalized to fragments per kilobase of exon model per million mapped reads (FPKM) using RNA-seq by Expectation Maximization (RSEM) (https://deweylab.github.io/RSEM/README.html, version 1.2.12, default parameters). Differentially expressed genes (DEGs) were identified using the PossionDis tool from BGI Genomics, which utilizes the Poisson distribution method. Significantly different genes were filtered with a false discovery rate (FDR) cutoff of 0.001 and a log-fold change (LogFC) threshold of 2. Genes with LogFC ≥ 2 or LogFC ≤ -2 and FDR ≤ 0.001 between two treatment conditions were classified as up-regulated and down-regulated, respectively. Functional and pathway analyses of 121 DEGs were conducted using the "limma" package. Gene Ontology (GO, http://geneontology.org/) and Kyoto Encyclopedia of Genes and Genomes (KEGG, https://www.kegg.jp/kegg/

Table 1 The Sequences of Primers Used in qPCR

Gene name	Forward Primer	Reverse Primer
m*PRKDC*	AGGGAAGAAGAGTCTCTGGTGG	ATTAGGGGATCTGTTGCCTGGC
m*IFNa*	GACCTTCCTCAGACTCATAACCT	TCCAAAGTCCTTCCTGTCCTT
m*IFNβ*	TCCGAGCAGAGATCTTCAGGAA	TGCAACCACCACTCATTCTGAG
m*ISG15*	CTGAAGAAGCAGATTGCCCAGAAG	CGCTGCAGTTCTGTACCACTAGC
m*ISG56*	TGGCCGTTTCCTACAGTT	TCCTCCAAGCAAAGGACTTC
m*CXCL10*	GCCGTCATTTTCTGCCTCA	CGTCCTTGCGAGAGGGATC
h*PRKDC*	CAGAGACGGTAATCACGGGT	TCGGAGTTGTTGGTCACAGA
	GCCCACCCTCTTGTACCTTC	GCTCCTACAGTTCTCTCGCC
h*IFNa*	GAGGAGTTTGATGGCAACCAG	GGTGCAGAATTTGTCTAGGAGGTC
h*IFNβ*	CAGGAGAGCAATTTGGAGGA	TGACATCTCAATTGCTCCAG
h*ISG15*	GAGCATCCTGGTGAGGAATAAC	CGCTCACTTGCTGCTTCA
h*ISG56*	GAAACTTCGGAGAAAGGCATTAG	CATAGTACTCCAGGGCTTCATT
h*CXCL10*	TGGCATTCAAGGAGTACCTC	TTGTAGCAATGATCTCAACACG
β-actin	GTTGTCAGCGACGAGCG	GCACAGAGCCTCGCCTT

kegg1.html) analyses were performed using the clusterProfiler (https://bioconductor.org/packages/release/bioc/html/clusterProfiler.html, version 3.6.0) R package (https://www.r-project.org/, version 3.4.4) for statistical enrichment analyses.

Immunofluorescence

The FADU, SCC7 and CAL27 cells were divided into four groups respectively: control (Ctr), cells treated with NU7441, cells treated with IR (10Gy), cells treated with NU7441 and IR (10Gy). After 4 hours, all cells were fixed with 4% paraformaldehyde for 15 minutes, permeabilized with 0.1% Triton X-100 for 10 minutes, and blocked with 2% bovine serum albumin in PBS for 1 hour at room temperature. Primary antibodies were incubated with the samples overnight at −4°C. After three washes, cells were incubated with Alexa Fluor 647-conjugated anti-mouse IgG H&L (Invitrogen, A-21202) and Alexa Fluor 568-conjugated anti-rabbit IgG H&L (Invitrogen, A-11012) for 1 hour at room temperature. Nuclei were stained with 4′,6-diamidino-2-phenylindole (DAPI) using Vectashield mounting medium. Images were then acquired using a Zeiss LSM700 confocal microscope and analyzed with a Zeiss LSM Image Browser.

Statistical Analysis

Statistical analysis was performed using GraphPad Prism software (GraphPad, La Jolla, CA, USA), with specific details provided in the figure legends.

Results

DNA-PK Inhibitor NU7441 Sensitizes Tumors to PD-1 Blockade and IR

This study aimed to assess whether NU7441 could enhance the efficacy of IR and ICIs in HNSCC tumors. Figure 1A illustrates the in vivo experimental process. To simulate a clinical setting, mice received various treatments: Control (Ctr), NU7441, Anti-PD1, IR with NU7441, IR, IR with Anti-PD1, Anti-PD1 with NU7441, and a triple therapy combining IR, Anti-PD1, and NU7441. The results showed similar effects on SCC7 tumor growth in the Anti-PD1, NU7441, and IR with NU7441 groups, while the IR and Anti-PD1 combination had minimal impact. Conversely, the triple therapy significantly reduced tumor growth, with a mean tumor volume of 195.9 mm^3 compared to 545.9 mm^3 in the Anti-PD1 with NU7441 group ($p<0.0001$; Figure 1B). Figure 1C presents dissected tumors on day 15, highlighting smaller volumes in the triple therapy group. The Ctr group showed an average survival time of 26 days, while the NU7441, Anti-PD1, and IR groups had average survival times of 26, 30, and 30 days respectively (Figure 1D). The triple therapy notably improved survival in the SCC7 model (Figure 1D). Adding NU7441 or Anti-PD1 to IR did not increase survival compared to IR alone (Supplementary Figure 1A). Including IR or Anti-PD1 with NU7441 did not significantly improve survival compared to NU7441 alone (Supplementary Figure 1B). Adding either IR or NU7441 to Anti-PD1 did not enhance survival rates. However, triple therapy significantly extended survival compared to IR alone or radioimmunotherapy (Supplementary Figure 1C). Incorporating NU7441 into radioimmunotherapy inhibited tumor growth and prolonged survival.

NU7441 Impacts T-Cell Infiltration Following Radioimmunotherapy

Given the superior antitumor effect of triple therapy compared to radioimmunotherapy, investigating NU7441's impact on the tumor immune microenvironment is crucial. Lymphocytes from tumors in eight groups were collected on day 15 (Figure 2A). Notably, the triple therapy group showed a significant increase in TIL CD8+ T cells compared to other groups (Figure 2B). In Figure 2C, the triple therapy group showed a significant increase in TIL CD4+ T cells compared to other groups except for the Ctr group and the IR+Nu7441 group. The addition of IR or NU7441 to Anti-PD1 did not significantly increase TIL CD8+ T cell quantities compared to the Anti-PD1 group alone (Supplementary Figure 2A). Similarly, adding IR or NU7441 to Anti-PD1 did not further augment TIL CD4+ T cell levels compared to Anti-PD1 alone (Supplementary Figure 2B). In contrast, while adding Anti-PD1 to IR did not significantly increase TIL CD4+ T cells, adding NU7441 to IR did result in a notable increase in TIL CD4+ T cell quantities (Supplementary Figure 2C). The addition of Anti-PD1 to NU7441 did not significantly increase TIL CD4+ T cells compared to NU7441 alone (Supplementary Figure 2D). However, the combination of IR and NU7441 led to a significant increase in TIL CD4+ T cells (Supplementary Figure 2D). This suggests that IR combined with NU7441 effectively stimulates the tumor immune microenvironment.

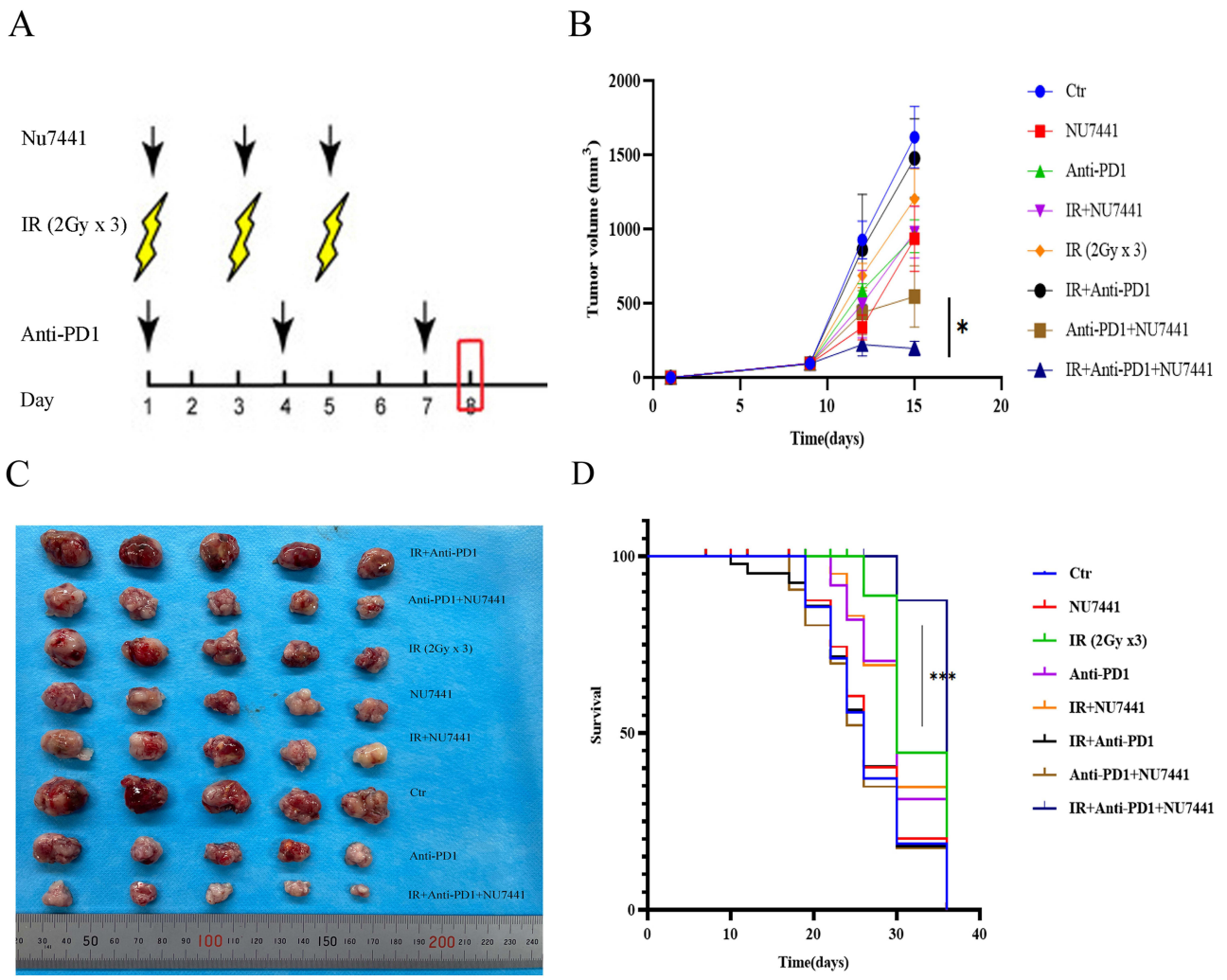

Figure 1 The inclusion of NU7441 enhances the efficacy of radiation therapy in conjunction with anti-PD-1 treatment, leading to improved control of tumor growth and increased survival rates in mice. (**A**) Schematic illustrating the sequential timelines of ionizing radiation (IR), NU7441 administration, and anti-PD-L1 treatment. The red box indicates the time point at which the tumor samples are collected. (**B-C**) The reaction exhibited by the subcutaneous tumors to the indicated treatment regimens. N=5 in each group. Data represent the mean±SEM. (**D**) The survival plots depicting the outcomes of each treatment regimen were presented. n=5 in each group. Data represent the mean±SEM. *p<0.05, ***p<0.001 (one-way ANOVA, with Dunnett's correction).

GO and KEGG Analyses of RNA-Seq Data

DNA-PKcs dysfunction enhances the antitumor activity of radioimmunotherapy in HNSCC, prompting further investigation into the underlying mechanisms. The cGAS-STING pathway, a well-established innate signaling pathway,[28] is known to synergize with Anti-PD1 therapy.[29] To explore the mechanisms driving the activation of downstream inflammatory factors in cGAS-STING signaling across various subgroups, this phenomenon was analyzed in *PRKDC* KD cells. Analysis revealed a notable increase in genes related to the cellular immune response in *PRKDC* KD FADU cells upon exposure to IR (Figure 3A). In *PRKDC* KD cell groups, IR induced upregulation of *MMP9* and *NLRP3*, as shown in the volcano map (Figure 3A). Figure 3B illustrates the up- and down-regulated genes in the IR combined with NU7441 group versus the Control group. In wild-type cells treated with NU7441, a comparison with IR combined with NU7441 revealed upregulation of *CD274* and *ULBP1* (Figure 3C). Similarly, IR combined with NU7441, when compared to wild-type cells treated with IR, showed both downregulation and upregulation of genes (Figure 3D). GO analysis compared the *PRKDC* KD group with the *PRKDC* KD combined with IR group, revealing upregulation of terms such as DNA replication-dependent nucleosome assembly and antimicrobial humoral immune response (Figure 3E). GO analysis (Figure 3F–H) also showed that compared to the Control, NU7441, and IR groups, NU7441 combined with IR

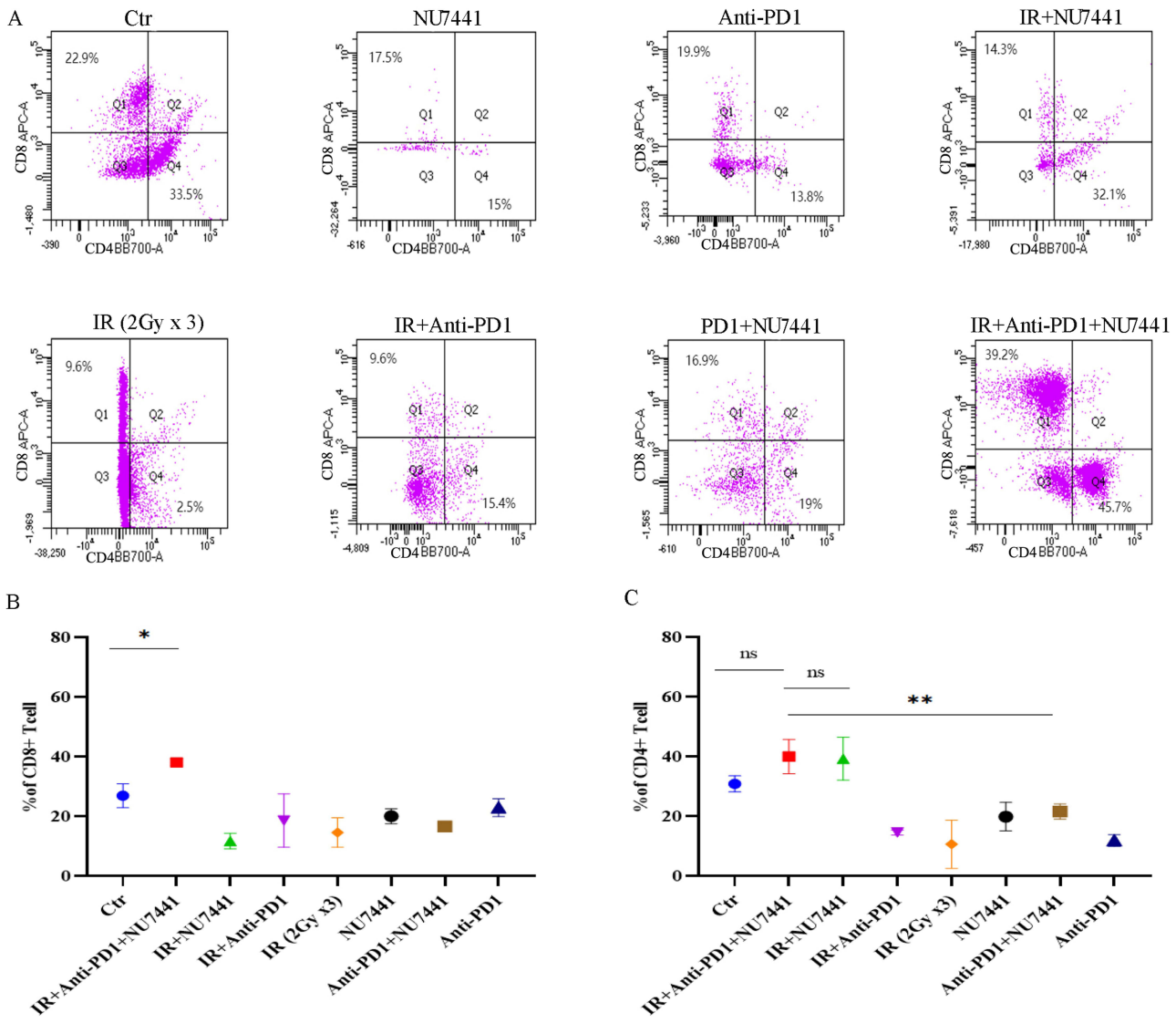

Figure 2 Triple therapy affects T cell infiltration in mice tumors. (**A**) Representative scatter plots depicting the percentages of tumor-infiltrating (TIL) Tcell (CD8+ T cell and CD4+ T cell). (**B**) The quantitation of the percentages of TIL CD8+ Tcell was shown in the different subgroups. Data represent the mean±SEM. (**C**) The quantitation of the percentages of TIL CD4+ Tcell was shown in the different subgroups. Data represent the mean±SEM. *p<0.05, **p<0.01, (one-way ANOVA, with Dunnett's correction). Ns, not significant (significance level, $\alpha = 0.05$).

group exhibited enrichment of upregulated terms, including immune system process and immune response. KEGG enrichment analysis revealed upregulation of the IL-17 signaling pathway, cytokine-cytokine receptor interaction, and Human T-cell leukemia virus 1 infection in the *PRKDC* KD combined with IR group compared to *PRKDC* KD cells (Figure 3I). Compared to the Control, NU7441, and IR groups, the NU7441 combined with IR group, KEGG analysis indicated enrichment of upregulated terms, including the cGMP-PKG signaling pathway and cAMP signaling pathway (Figure 3J–L). These findings suggest that *PRKDC* alteration or DNA-PK dysfunction activates immune-related pathways in response to radiation therapy.

DNA-PK Dysfunction Combined With IR Promotes Innate Immunity and Activates the cGAS-STING Pathway

Alterations in immune pathways, all of which were ISGs, were identified. The RNA-seq results were subsequently confirmed. We performed *PRKDC* gene lentiviral interference on FADU and CAL27 cells. At 72 hours after the lentiviral transfection of the cell strain, fluorescence microscopy revealed a higher number of black and green GFP-positive cells in

https://doi.org/10.2147/JIR.S497295

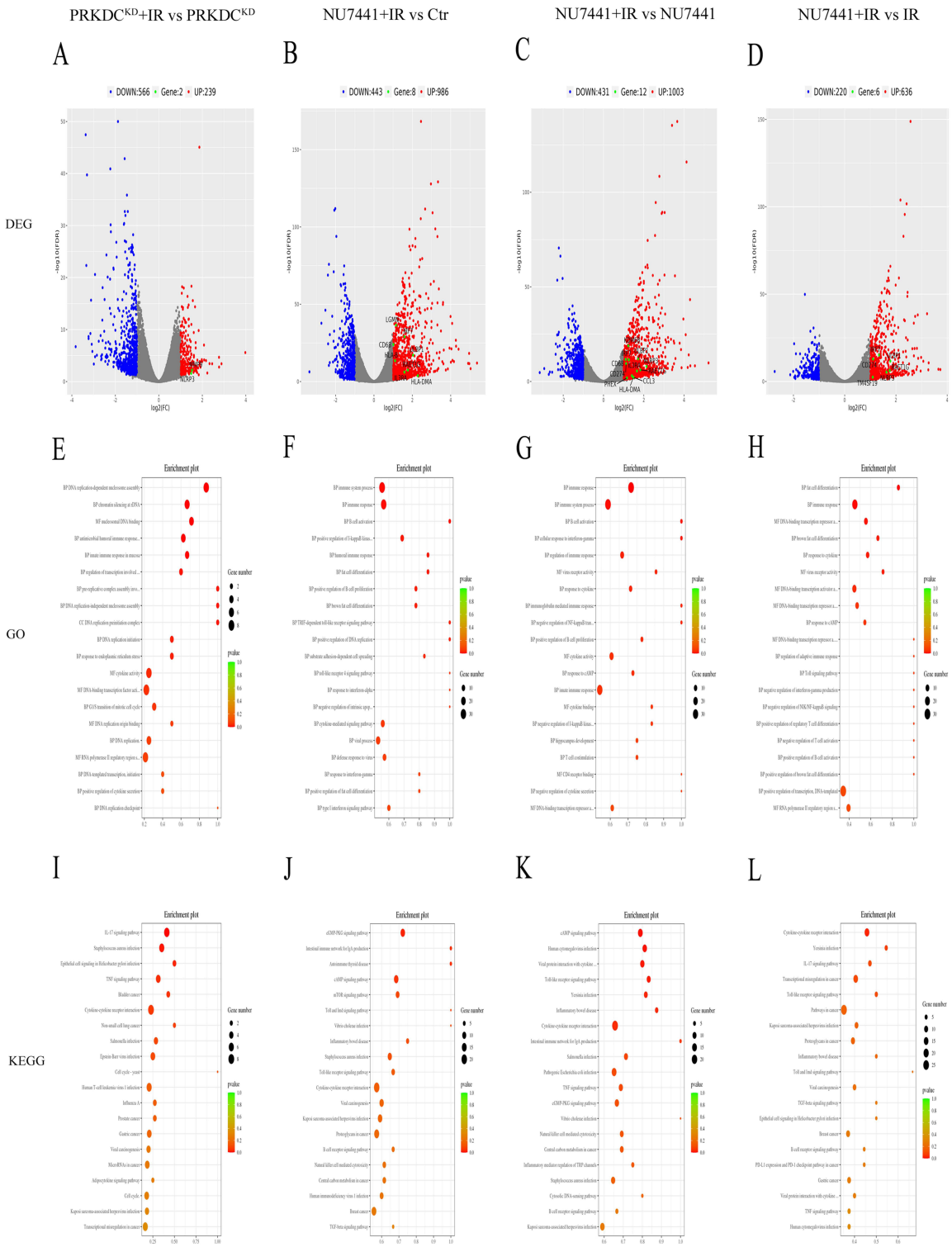

Figure 3 NU7441 combined with radiotherapy activates immune-related pathways using RNA-seq analyses. (**A-D**) Volcano plot of differentially expressed genes in the different subgroups in FADU cells. (**A**) *PRKDC*^{KD} combined with radiotherapy subgroup vs *PRKDC*^{KD} subgroup. (**B**) NU7441 combined with radiotherapy subgroup vs wild-type subgroup. (**C**) NU7441 combined with radiotherapy subgroup vs NU7441 subgroup. (**D**) NU7441 combined with radiotherapy subgroup vs radiotherapy subgroup. Gene Ontology analysis indicates significant enrichment of up-regulated terms in the *PRKDC*^{KD} combined with radiotherapy subgroup vs *PRKDC*^{KD} subgroup (**E**), NU7441 combined with radiotherapy subgroup vs wild-type subgroup (**F**), NU7441 combined with radiotherapy subgroup vs NU7441 subgroup (**G**), NU7441 combined with radiotherapy subgroup vs radiotherapy subgroup (**H**). Kyoto Encyclopedia of Genes and Genomes analysis indicates significant enrichment of up-regulated terms in the *PRKDC*^{KD} combined with radiotherapy subgroup vs *PRKDC*^{KD} subgroup (**I**), NU7441 combined with radiotherapy subgroup vs wild-type subgroup (**J**), NU7441 combined with radiotherapy subgroup vs NU7441 subgroup (**K**), NU7441 combined with radiotherapy subgroup vs radiotherapy subgroup (**L**). All samples were collected after 8 h after radiotherapy. Color gradient indicates fold changes in log2 scale.

CAL27 cells (Figure 4A) and FADU cells (Figure 4B) compared to wild-type (WT) cells following transfection, which indicates that the lentiviral transfection efficiency was relatively higher. The stable cell lines, in which DNA-PKcs expression was downregulated via shRNA, was generated from CAL27 and FADU cells (Figure 4C–D).This observation was confirmed by Western blot analysis (Figure 4C–D). Western blot analyses demonstrated that *PRKDC* KD resulted in the phosphorylation of TBK1 and IRF3 induced by IR in CAL27 cells (Figure 4E) and FADU cells (Figure 4F). Quantification of phosphorylation levels of TBK1 and IRF3 bands (Figure 4G–H) supported these findings. Based on these results, it is hypothesized that the deficiency of DNA-PK combined with IR might enhance innate immunity.

Western blot analyses demonstrated that administering NU7441 elevated TBK1 and IRF3 phosphorylation induced by IR in CAL27 wild-type cells (Figure 5A) and FADU wild-type cells (Figure 5B). Quantification of TBK1 and IRF3 phosphorylation levels (Figure 5D and E) supports this observation. In SCC7 wild-type cells, Western blot analyses revealed that NU7441 treatment resulted in increased TBK1 phosphorylation induced by IR, while no significant change was observed in IRF3 phosphorylation (Figure 5C and F).

PCR analyses revealed that NU7441 treatment significantly increased the expression of *IFNα, IFNβ, ISG15, ISG56*, and *CXCL10* induced by IR in wild-type CAL27 cells (Figure 6A), FADU cells (Figure 6C), and SCC7 cells (Figure 6E). Additionally, the induction of *IFNα, IFNβ, ISG15, ISG56*, and *CXCL10* was enhanced in CAL27 cells (Figure 6B) and FADU cells (Figure 6D) when *PRKDC* KD stable cells were treated with IR.

Release of Cytosolic dsDNA Is Responsible for DNA-PKcs Inhibition Combined With IR-Induced Activation of the cGAS-STING Pathway

To determine if cGAS-STING pathway activation was caused by dsDNA breaks, confocal experiments were performed with dsDNA and γH2AX. H2A.X is crucial for cell cycle arrest and DNA repair after DNA damage,[30] rapidly phosphorylating at Ser139 by DNA-PK in response to IR.[31] DNA-PKcs dysfunction resulted in an increased sensitivity to radiation and decreased repair of DNA double-strand breaks (DSB) (Figure 7A–D). After 10 Gy, the level of γH2AX in CAL27 and FADU cells was quickly elevated, reaching a peak at about 4 h post-irradiation. The γH2AX phosphorylation foci and dsDNA expression were visualized in CAL27, SCC7, and FADU cells (Figure 7A–D). In DMSO-treated control cells, the formation of γH2AX foci and dsDNA per cell exhibited a notably low level of background focus, which was not significantly increased by NU7441 or IR alone in cells (Figure 7A–D). However, simultaneous treatment with NU7441 and IR significantly increased both the quantity of γH2AX foci and the expression level of dsDNA (Figure 7A–D). Fluorescent intensity of dsDNA (Supplementary Figure 3A) for NU7441+IR group was 2.82±0.89/mm^2. Fluorescent intensity of dsDNA (Supplementary Figure 3A) for Ctr, NU7441, and IR group were 1.55±0.52/mm^2, 1.09±0.36/mm^2, 1.23±0.39/mm^2, respectively. Foci count of gamma-H2AX (Supplementary Figure 3B) for NU7441+IR group was (6.35±1.92)×10^4 foci /mm^2. Foci count of gamma-H2AX (Supplementary Figure 3B) for Ctr, NU7441, and IR group were (4.76±1.59)×10^3 foci /mm^2, (1.36±0.43)×10^4 foci /mm^2, (4.41±1.39)×10^4 foci /mm^2, respectively. Quantitative assessment of immunostaining for foci count of gamma-H2AX and fluorescent intensity of dsDNA showed higher quantity in NU7441+IR group. Therefore, these data indicate that DNA-PKcs plays a critical role in the phosphorylation of H2AX in response to DNA damage.

Discussion

In this study, the combined treatment of RT and immunotherapy did not significantly impact tumor growth control or survival prolongation in mice. Research indicates that low-dose X-ray therapy can improve the TME, facilitating better immune cell infiltration.[32,33] Preclinical and clinical trials have demonstrated that low-dose irradiation plays a crucial role in treating metastatic tumors by enhancing T-cell function and combating cancer.[34,35] However, the combination of RT and immunotherapy only resulted in a modest increase in efficacy, with a success rate of merely 40%.[36] IR-induced changes have been shown to negatively affect the immune response by enhancing signaling pathways in the TME and upregulating inhibitory cellular functions, leading to tumor immune evasion.[37] Previous research[38] has demonstrated that RT induces an increase in M2 macrophages and Treg cells within the TME, both of which negatively regulate anti-tumor immunogenicity. Consequently, strategies to improve the efficacy of radioimmunotherapy in HNSCC were explored.

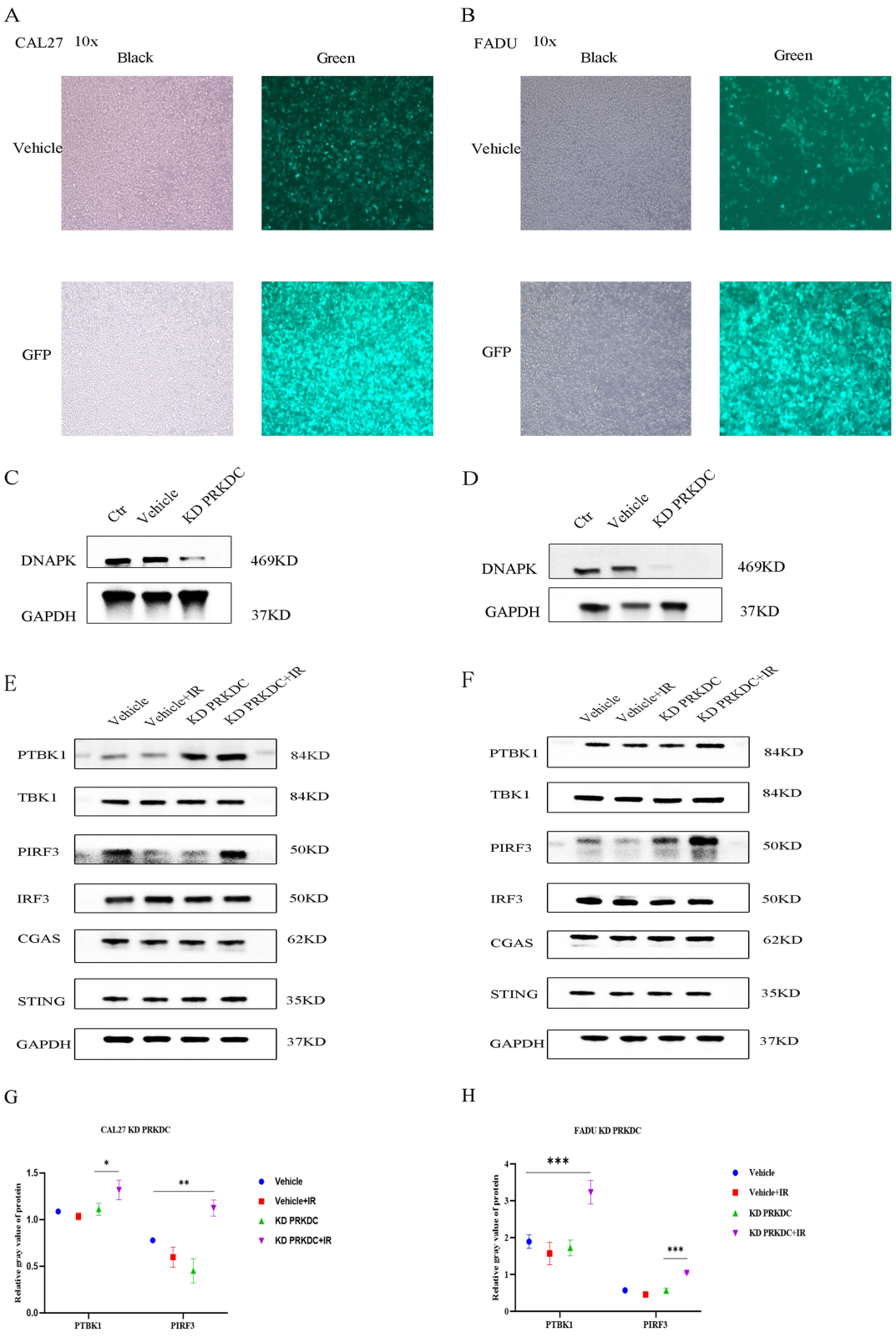

Figure 4 Knockdown of PRKDC activates the cGAS-STING pathway. (**A**) Fluorescence microscopy of GFP expression 24 hours after transfection of wild-type and PRKDC^{KD} CAL27 cells with increased fluorescence intensity. (**B**) Fluorescence microscopy of GFP expression 24 hours after transfection of wild-type and PRKDC^{KD} FADU cells with increased fluorescence intensity. (**C**) Western blot of DNAPK protein in wild-type or PRKDC^{KD} CAL27 cells. (**D**) Western blot of DNAPK protein in wild-type or PRKDC^{KD} FADU cells. (**E**) Western blot of PTBK1, TBK1, PIRF3, IRF3, CGAS, and STING proteins in the different subgroups in CAL27 cells. (**F**) Western blot of PTBK1, TBK1, PIRF3, IRF3, CGAS, and STING proteins in the different subgroups in FADU cells. (**G-H**) Expression levels of PTBK1 and PIRF3 in the different subgroups following transfection of lentivirus into CAL27 cells (**G**), FADU cells (**H**). Data represent the mean±SEM. *p<0.05, **p<0.01, ***p<0.001 (one-way ANOVA, with Dunnett's correction).

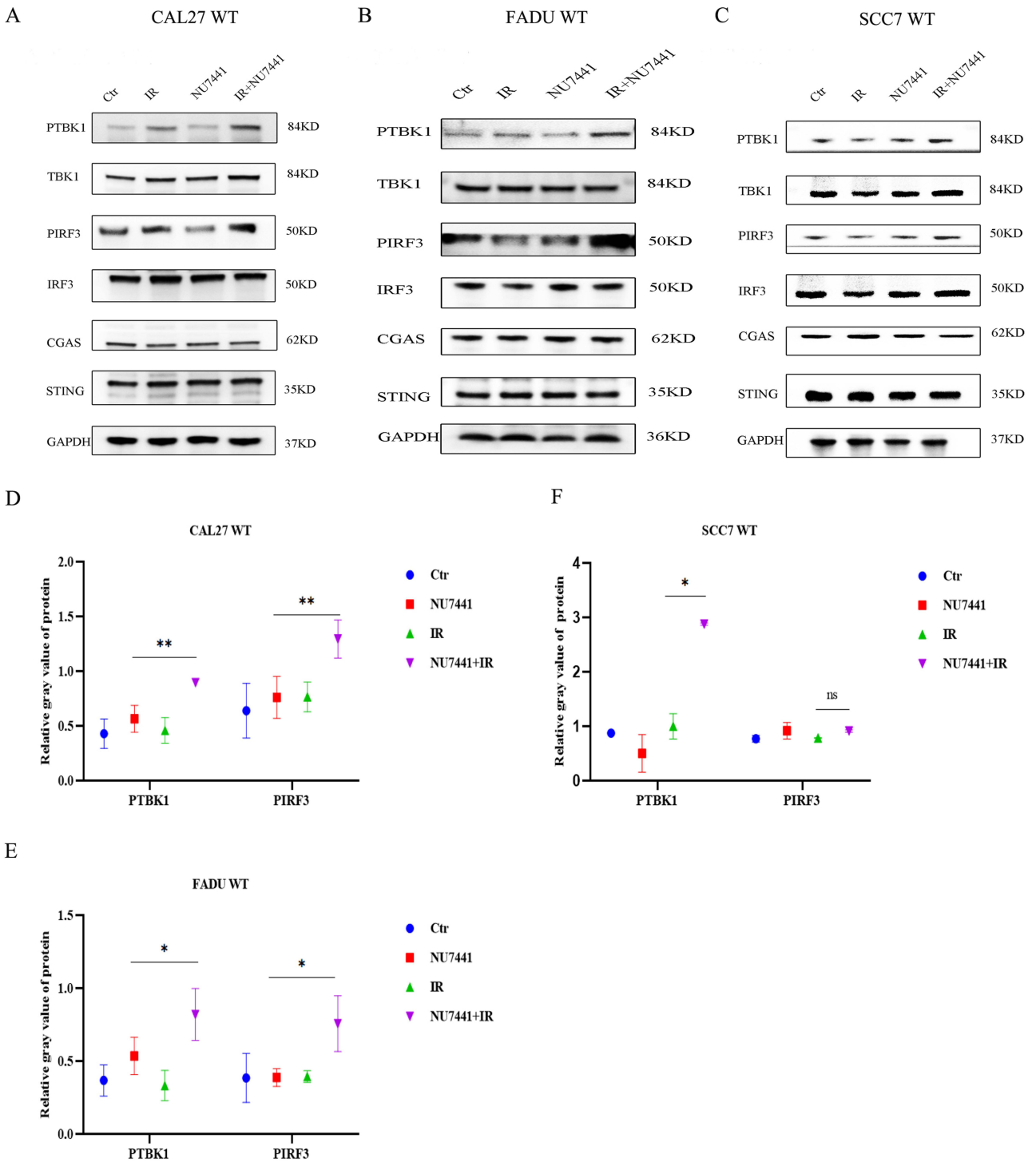

Figure 5 DNA-PK inhibitor combined with radiotherapy promotes innate immunity and activates the cGAS-STING pathway. (**A-C**) Western blot of PTBK1, TBK1, PIRF3, IRF3, CGAS, and STING proteins in the different subgroups in CAL27 cells (**A**), FADU cells (**B**), and SCC7 cells (**C**). (**D, E**) Expression levels of PTBK1 and PIRF3 in the different subgroups of CAL27 cells (**D**), FADU cells (**E**). (**F**) Expression levels of PTBK1 in the different subgroups in SCC7 cells. Data represent the mean±SEM. *p<0.05, **p<0.01, (one-way ANOVA, with Dunnett's correction). Ns, not significant (significance level, $\alpha = 0.05$).

Because NHEJ is the primary pathway for IR-induced DNA repair,[39] using DNA-PK inhibitors like NU7441 can sensitize tumors to IR and prevent IR-induced DNA repair. Combining NU7441 with radioimmunotherapy improved tumor control and prolonged survival in mice. Consequently, modifications within the tumor immune microenvironment were investigated following the combined treatment. A notable increase in CD8+ T and CD4+ T cells was observed in

https://doi.org/10.2147/JIR.S497295

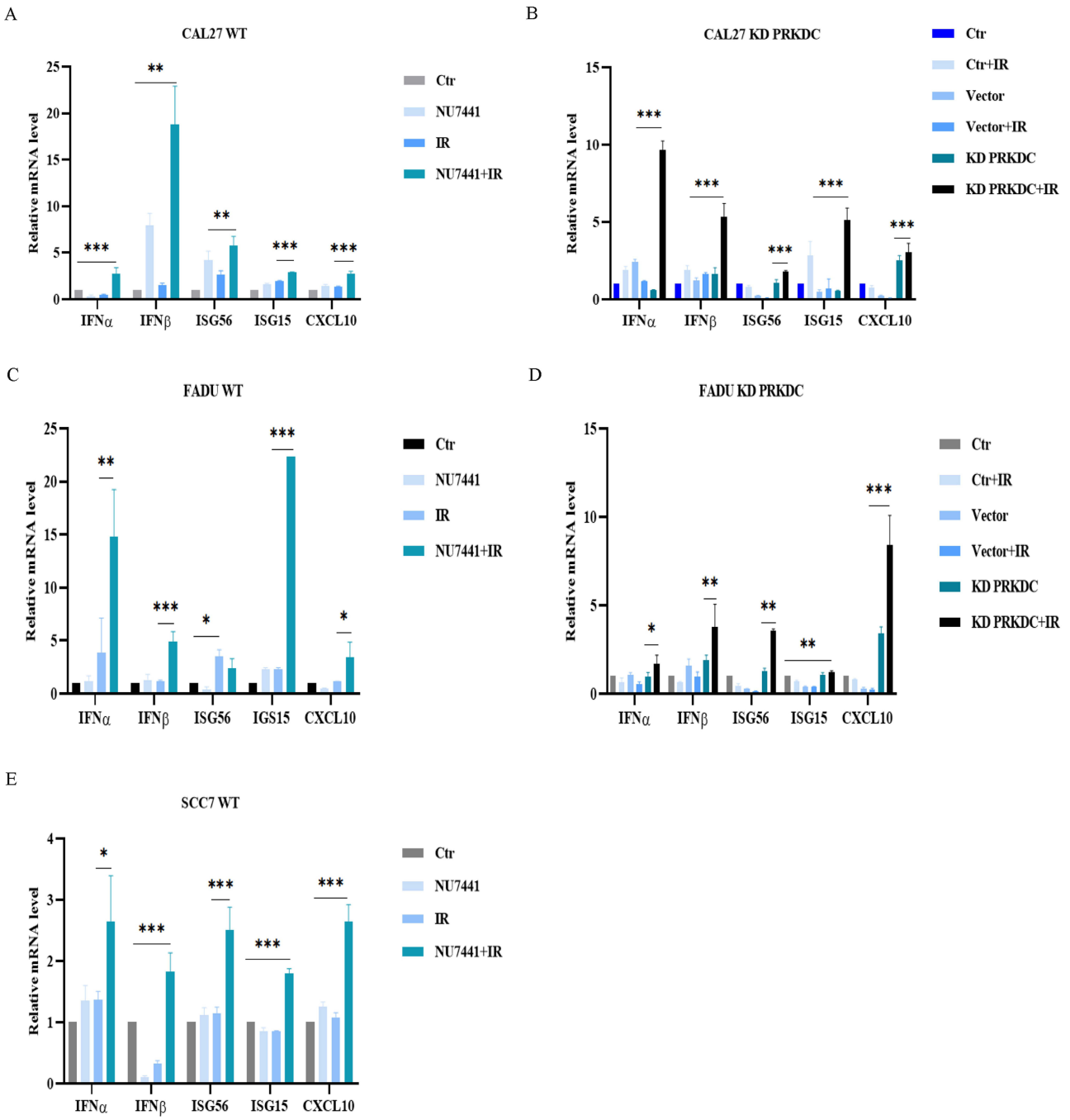

Figure 6 DNA-PK deficiency combined with radiotherapy activates the inflammatory factors downstream of interferon. (**A, C, E**) Expression of IFNα, IFNβ, ISG56, ISG15, and CXCL10 were measured using RT-qPCR in the different subgroups of wild-type CAL27 cells (**A**), FADU cells (**C**), and SCC7 cells (**E**). (**B, D**) Expression of IFNα, IFNβ, ISG56, ISG15, and CXCL10 were measured using RT-qPCR in the different subgroups of PRKDC KD CAL27 cells (**B**), FADU cells (**D**). Data represent the mean±SEM. *p<0.05, **p<0.01, ***p<0.001 (one-way ANOVA, with Dunnett's correction).

tumor-infiltrating lymphocytes among subjects receiving the three combination regimen compared to other groups. This supported the idea that immune cell composition and characteristics in the TME were crucial for determining the response to ICIs.[40] Patients with immunothermal tumors showing PD-L1, CD4+, and CD8+ T cells near tumor cells respond better to anti-PD-L1/PD-1 therapy than those lacking these effector populations or with an "immune-exclusion" phenotype.[41] Low T cell infiltration is associated with a negative prognosis[42] and an inadequate response to cancer immunotherapy[43] in numerous human malignancies. CD8+ T cells use major histocompatibility complex (MHC) class

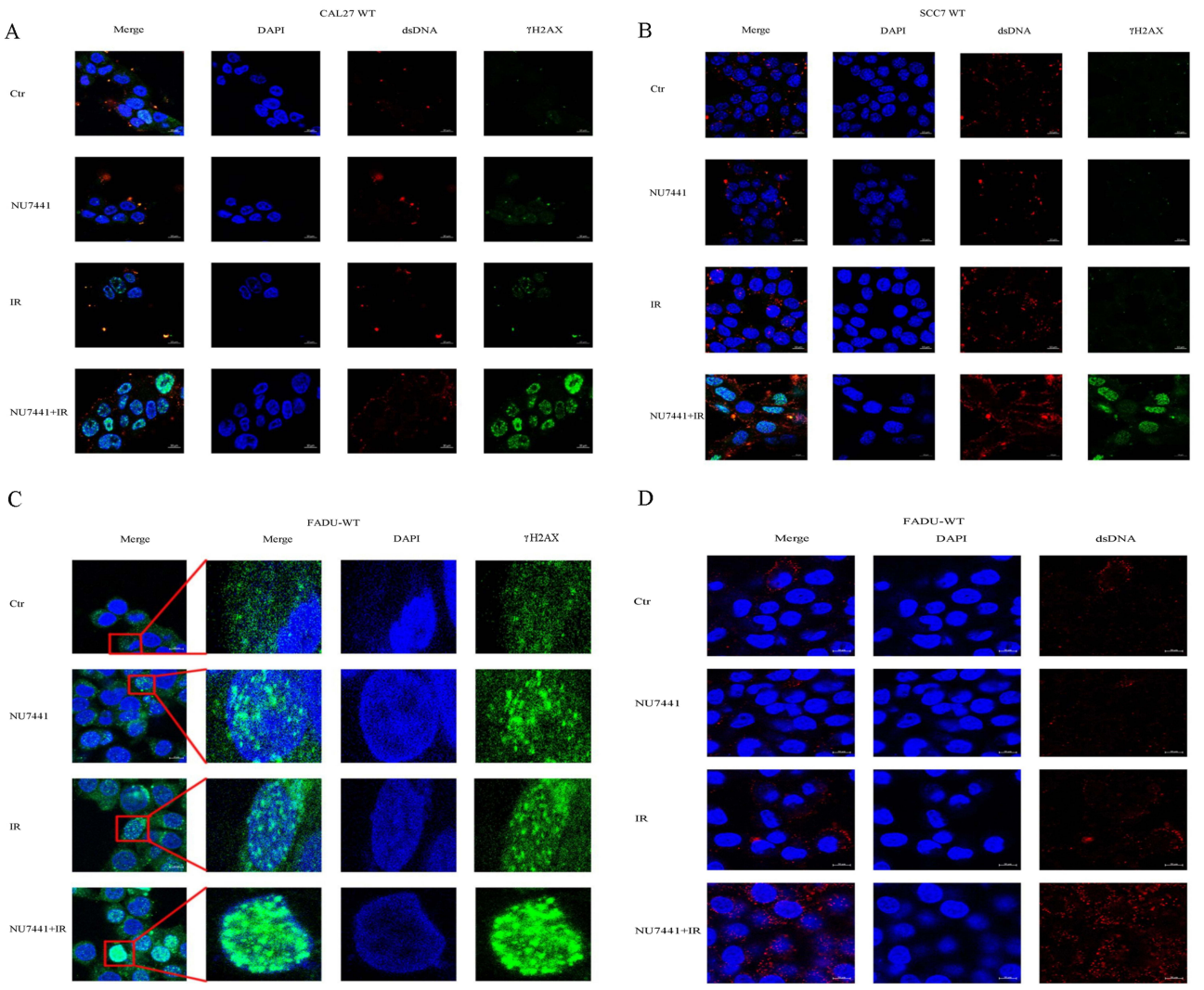

Figure 7 Release of cytosolic dsDNA is responsible for PRKDC inhibition deficiency combined with radiotherapy-induced activation of the cGAS-STING pathway. (**A**) CAL27 cells, (**B**) SCC7 cells, FADU cells (**C-D**) were then subjected to immunofluorescence analysis (dsDNA (red), (γH2AX (green)), and (4′,6-diamidino-2-phenylindole (DAPI)(bule)).

I molecules to target and destroy cancer cells, while CD4+ T cells also help fight tumors.[44] CD4+ T cells are necessary for activating CD8+ T cells, helping maintain their ability to kill infected cells.[45,46] The recruitment of innate immune cells, particularly dendritic cells, play a critical role in antigen presentation and T-cell activation. We observed T-cell infiltration induced by NU7441+ in the mouse model, but further study is needed to determine if innate immune cells like dendritic cells are attracted to the tumor TME. While the current study focuses on CD4+ and CD8+ T cells due to their well-established roles in antitumor immunity and the scope of our experimental design, it is useful that expanding the characterization of the TME would be beneficial. In future work, we plan to incorporate a more thorough analysis, including other immune cell populations (eg, Tregs, macrophages, NK cells) and non-cellular components of the TME.

DNA-PK dysfunction combined with radioimmunotherapy exhibits significant efficacy, prompting exploration of the underlying mechanisms through RNA-Seq analysis. Single-cell sequencing revealed that *PRKDC* gene alterations promote the expression of *NLRP3* (NOD-like receptor family pyrin domain containing 3), consistent with previous studies.[47] *NLRP3* agonists can enhance antigen presentation and promote T cell priming, thus facilitating radiation-induced immune priming in an anti-PD1 resistance model.[45] Additionally, our results showed that NU7441 significantly upregulated IR-induced *LGMN* (Legumain), *CD274, HLA-DMA*, and *ULBP1* (UL16-binding protein 1). Previous studies[48] have indicated that increased *LGMN* promotes tumor-induced immunosuppressive polarization of tumor-associated macrophages by activating the GSK-

https://doi.org/10.2147/JIR.S497295

3β-STAT3 signaling pathway, enhances CD8+ T cell-mediated anti-tumor immunity, and produces synergistic effects with anti-PD-1 therapy. The protein encoded by the *CD274* gene is PD-L1. In our study, inhibiting DNA-PK function increased *CD274* gene expression by IR, supporting the rationale for enhanced immunotherapy efficacy with NU7441 combined with IR. *HLA-DMA*, an antigen presentation-related gene, has expression levels correlated with specific T-cell infiltration and immunotherapy efficacy.[49] The protein encoded by the *ULBP1* gene is a ligand for *NKG2D* (natural killer cell D member). In HNSCC, *ULBP1* expression levels are positively correlated with patient survival, and upregulation of human *NKG2D* ligand *ULBP1* on tumor cells enhances NK cell-mediated killing.[50] *ULBP1* has been confirmed as a biomarker in different lymphoma patients, predicting responsiveness to T cell immunotherapy.[51] CAR-T therapy targeting *NKG2D* ligands has shown superior antitumor effects and safety in preclinical and clinical trials.[52] GO analysis revealed that *PRKDC* genetic alteration or DNA-PK function inhibition promotes DNA replication-dependent nucleosome assembly, antimicrobial humoral immune response, immune system processes, and immune response. KEGG analysis showed that *PRKDC* genetic alteration or DNA-PK function inhibition enriched IR effects on the cGMP-PKG signaling pathway, cAMP signaling pathway, IL-17 signaling pathway, cytokine-cytokine receptor interaction, and Human T-cell leukemia virus 1 infection. Together, these results suggested that genetic alteration in *PRKDC* or inhibition of DNA-PK function leads to the activation of immune-related genes and inflammatory cytokines upon exposure to IR. NU7441 combined with RT has the potential to stimulate the tumor immune microenvironment, forming the basis for combined immunotherapy.

Alterations in immune pathways, specifically ISGs, were identified and confirmed through qPCR and Western blotting. Considering the potential activation of the cGAS-STING pathway, changes in TBK1 and IRF3 were examined, revealing pathway activation. Our data indicate that combining NU7441 with IR enhances double-stranded DNA breaks, and that dsDNA binding to cGAS activates the cGAS-STING pathway. This provides strong evidence for *PRKDC*'s role in repairing IR-induced DNA damage in tumor cells. Therefore, targeting cellular pathways responsible for DNA damage repair is crucial for modulating tumor therapy efficacy. Further comprehensive exploration of the molecular mechanisms underlying the DNA damage response will inform the development of clinical approaches for treating tumors.

There are several limitations to this study. First, the reduced antitumor effect of the combination therapy (IR+anti-PD-1) compared to individual treatments may stem from several factors: suboptimal dosing and timing of IR and anti-PD-1, potential IR-induced immunosuppression, tumor heterogeneity, or model-specific characteristics. These limitations underscore the need for further optimization of the combination therapy and a deeper exploration of the post-IR immune microenvironment to clarify its impact on anti-PD-1 efficacy. Addressing these issues in future studies may offer more definitive insights into the therapeutic potential of this approach. Second, we aim to investigate whether specific genes and pathways exhibit expression changes under certain conditions and their potential functional roles, thereby influencing the therapeutic outcomes across different subgroups. Therefore, validating the gene expressions mentioned in Figure 3 is crucial. We plan to address this in future studies. Third, the immune response observed in our model may not fully replicate the neoantigen-driven T-cell response seen in human tumors. Therefore, future studies should use humanized mouse models or patient-derived xenografts to better replicate human immune responses. Additionally, clinical studies will be essential to confirm the therapeutic potential of NU7441 in combination with immunotherapy in human patients.

Conclusion

In summary, our study demonstrated that the combination of NU7441, IR, and Anti-PD-1 in a mouse model of HNSCC exhibited significantly superior efficacy compared to monotherapy or pairwise combination therapies. Specifically, *PRKDC* genetic alteration or DNA-PK dysfunction enhanced IR-induced cellular DNA breaks, leading to the phosphorylation of TBK1 and IRF3, activation of the cGAS-STING pathway, reconstruction of the TME, and an enhanced anti-tumor immune response.

Data Sharing Statement

All data generated or analyzed during this study are included in this published article. The data presented in this study are available on request from the corresponding author.

Consent for Publication

All authors approved the final version of the manuscript.

Ethics Statement

All mice studied in our research were cared in accordance with Clinical Oncology School of Fujian Medical University institution guidelines. Ethical approval was sought from Clinical Oncology School of Fujian Medical University / Fujian Cancer Hospital Ethics Committee prior to commencing this study.

Funding

This work was supported by The Natural Science Foundation of Fujian Province, China (Grant No. 2022J011054, 2023J011254); Joint Funds for the Innovation of Science and Technology, Fujian province (Grant No. 2024Y9616, 2023Y9412); Young and Middle-aged Scientific Research Major Project of Fujian Provincial Health Commission (Grant No. 2022ZQNZD009); the Special Research Funds for Local Science and Technology Development Guided by Central Government (2023L3020); National Natural Science Foundation of China (Grant No. 82350126); the Fujian Medical University Student Innovation and EntrepreneurshipTraining Project,China (Grant No.202410392008).

Disclosure

The authors declare that the research was conducted in the absence of any commercial or financial relationships that could be construed as a potential conflict of interest.

References

1. Siegel RL, Miller KD, Wagle NS, Jemal A. Cancer statistics, 2023. *Ca a Cancer J Clinicians*. 2023;73(1):17–48. doi:10.3322/caac.21763
2. Semrau R. The role of radiotherapy in the definitive and postoperative treatment of advanced head and neck cancer. *Oncol Res Treatment*. 2017;40 (6):347–352. doi:10.1159/000477128
3. Feng RM, Zong YN, Cao SM, Xu RH. Current cancer situation in China: good or bad news from the 2018 Global Cancer Statistics? *Cancer Commun*. 2019;39(1):22. doi:10.1186/s40880-019-0368-6
4. Jones TM, De M, Foran B, Harrington K, Mortimore S. Laryngeal cancer: United Kingdom national multidisciplinary guidelines. *J Laryngology Otol*. 2016;130(S2):S75–s82. doi:10.1017/S0022215116000487
5. Saba NF, Blumenschein G Jr, Guigay J, et al. Nivolumab versus investigator's choice in patients with recurrent or metastatic squamous cell carcinoma of the head and neck: efficacy and safety in CheckMate 141 by age. *Oral Oncol*. 2019;96:7–14. doi:10.1016/j.oraloncology.2019.06.017
6. Szturz P, Vermorken JB. Translating KEYNOTE-048 into practice recommendations for head and neck cancer. *Ann translat Med*. 2020;8(15):975. doi:10.21037/atm.2020.03.164
7. McCaw ZR, Ludmir EB, Kim DH, Wei LJ. Further clinical interpretation and implications of KEYNOTE-048 findings. *Lancet*. 2020;396 (10248):378–379. doi:10.1016/S0140-6736(20)30904-1
8. Burnette BC, Liang H, Lee Y, et al. The efficacy of radiotherapy relies upon induction of type i interferon-dependent innate and adaptive immunity. *Cancer Res*. 2011;71(7):2488–2496. doi:10.1158/0008-5472.CAN-10-2820
9. Ghosh-Laskar S, Kalyani N, Gupta T, et al. Conventional radiotherapy versus concurrent chemoradiotherapy versus accelerated radiotherapy in locoregionally advanced carcinoma of head and neck: results of a prospective randomized trial. *Head Neck*. 2016;38(2):202–207. doi:10.1002/hed.23865
10. Choi JS, Sansoni ER, Lovin BD, et al. Abscopal effect following immunotherapy and combined stereotactic body radiation therapy in recurrent metastatic head and neck squamous cell carcinoma: a report of two cases and literature review. *Ann Otology Rhinology Laryngology*. 2020;129 (5):517–522. doi:10.1177/0003489419896602
11. Wu JS, Jen CW, Chen HH, Cheng SH. Stereotactic body radiotherapy and checkpoint inhibitor for locally recurrent unresectable nasopharyngeal carcinoma. *BMJ Case Rep*. 2021;14(7):e240806. doi:10.1136/bcr-2020-240806
12. Akbor M, Hung KF, Yang YP, et al. Immunotherapy orchestrates radiotherapy in composing abscopal effects: a strategic review in metastatic head and neck cancer. *J Chin Med Assoc*. 2020;83(2):113–116. doi:10.1097/JCMA.0000000000000234
13. McBride S, Sherman E, Tsai CJ, et al. Randomized Phase II trial of nivolumab with stereotactic body radiotherapy versus nivolumab alone in metastatic head and neck squamous cell carcinoma. *J Clin Oncol*. 2021;39(1):30–37. doi:10.1200/JCO.20.00290
14. Yu Y, Lee NY. JAVELIN head and neck 100: a phase III trial of avelumab and chemoradiation for locally advanced head and neck cancer. *Future Oncol*. 2019;15(7):687–694. doi:10.2217/fon-2018-0405
15. Sato H, Niimi A, Yasuhara T, et al. DNA double-strand break repair pathway regulates PD-L1 expression in cancer cells. *Nat Commun*. 2017;8 (1):1751. doi:10.1038/s41467-017-01883-9
16. Yue X, Bai C, Xie D, Ma T, Zhou PK. DNA-PKcs: a multi-faceted player in DNA damage response. *Front Genetics*. 2020;11:607428. doi:10.3389/fgene.2020.607428
17. Yang L, Liu Y, Sun C, et al. Inhibition of DNA-PKcs enhances radiosensitivity and increases the levels of ATM and ATR in NSCLC cells exposed to carbon ion irradiation. *Oncol Lett*. 2015;10(5):2856–2864. doi:10.3892/ol.2015.3730
18. Zhao Y, Thomas HD, Batey MA, et al. Preclinical evaluation of a potent novel DNA-dependent protein kinase inhibitor NU7441. *Cancer Res*. 2006;66(10):5354–5362. doi:10.1158/0008-5472.CAN-05-4275
19. Leahy JJ, Golding BT, Griffin RJ, et al. Identification of a highly potent and selective DNA-dependent protein kinase (DNA-PK) inhibitor (NU7441) by screening of chromenone libraries. *Bioorg. Med. Chem. Lett.* 2004;14(24):6083–6087. doi:10.1016/j.bmcl.2004.09.060
20. Cruet-Hennequart S, Coyne S, Glynn MT, Oakley GG, Carty MP. UV-induced RPA phosphorylation is increased in the absence of DNA polymerase eta and requires DNA-PK. *DNA Repair*. 2006;5(4):491–504. doi:10.1016/j.dnarep.2006.01.008

21. Robert F, Barbeau M, Éthier S, Dostie J, Pelletier J. Pharmacological inhibition of DNA-PK stimulates Cas9-mediated genome editing. *Genome Med*. 2015;7(1):93. doi:10.1186/s13073-015-0215-6
22. Sun X, Liu T, Zhao J, et al. DNA-PK deficiency potentiates cGAS-mediated antiviral innate immunity. *Nat Commun*. 2020;11(1):6182. doi:10.1038/s41467-020-19941-0
23. Carr MI, Chiu LY, Guo Y, et al. DNA-PK inhibitor peposertib amplifies radiation-induced inflammatory micronucleation and enhances TGFβ/PD-L1 targeted cancer immunotherapy. *mol Cancer Res*. 2022;20(4):568–582. doi:10.1158/1541-7786.MCR-21-0612
24. Sheng H, Huang Y, Xiao Y, et al. ATR inhibitor AZD6738 enhances the antitumor activity of radiotherapy and immune checkpoint inhibitors by potentiating the tumor immune microenvironment in hepatocellular carcinoma. *J Immunotherapy Cancer*. 2020;8(1):e000340. doi:10.1136/jitc-2019-000340
25. Chen Y, Li Y, Guan Y, et al. Prevalence of PRKDC mutations and association with response to immune checkpoint inhibitors in solid tumors. *Mol oncol*. 2020;14(9):2096–2110. doi:10.1002/1878-0261.12739
26. Luo P, Zhao Y, Li D, et al. Protective effect of Homer 1a on tumor necrosis factor-α with cycloheximide-induced apoptosis is mediated by mitogen-activated protein kinase pathways. *Apoptosis*. 2012;17(9):975–988. doi:10.1007/s10495-012-0736-z
27. Lv Q, Wang G, Zhang Y, et al. FABP5 regulates the proliferation of clear cell renal cell carcinoma cells via the PI3K/AKT signaling pathway. *Int J Oncol*. 2019;54(4):1221–1232. doi:10.3892/ijo.2019.4721
28. Chen Q, Sun L, Chen ZJ. Regulation and function of the cGAS-STING pathway of cytosolic DNA sensing. *Nat Immunol*. 2016;17(10):1142–1149. doi:10.1038/ni.3558
29. Wang H, Hu S, Chen X, et al. cGAS is essential for the antitumor effect of immune checkpoint blockade. *Proc Natl Acad Sci USA*. 2017;114 (7):1637–1642. doi:10.1073/pnas.1621363114
30. Yuan J, Adamski R, Chen J. Focus on histone variant H2AX: to be or not to be. *FEBS Lett*. 2010;584(17):3717–3724. doi:10.1016/j.febslet.2010.05.021
31. Burma S, Chen BP, Murphy M, Kurimasa A, Chen DJ. ATM phosphorylates histone H2AX in response to DNA double-strand breaks. *J Biol Chem*. 2001;276(45):42462–42467. doi:10.1074/jbc.C100466200
32. Herrera FG, Ronet C, Ochoa de Olza M, et al. Low-dose radiotherapy reverses tumor immune desertification and resistance to immunotherapy. *Cancer Discovery*. 2022;12(1):108–133. doi:10.1158/2159-8290.CD-21-0003
33. Grudzinski JJ, Hernandez R, Marsh I, et al. Preclinical characterization of (86/90)Y-NM600 in a variety of murine and human cancer tumor models. *J Nuclear Med*. 2019;60(11):1622–1628. doi:10.2967/jnumed.118.224808
34. Barsoumian HB, Ramapriyan R, Younes AI, et al. Low-dose radiation treatment enhances systemic antitumor immune responses by overcoming the inhibitory stroma. *Journal for Immunotherapy of Cancer*. 2020;8(2):e000537. doi:10.1136/jitc-2020-000537
35. Klug F, Prakash H, Huber PE, et al. Low-dose irradiation programs macrophage differentiation to an iNOS^{+}/M1 phenotype that orchestrates effective T cell immunotherapy. *Cancer Cell*. 2013;24(5):589–602. doi:10.1016/j.ccr.2013.09.014
36. Menon H, Ramapriyan R, Cushman TR, et al. Role of radiation therapy in modulation of the tumor stroma and microenvironment. *Front Immunol*. 2019;10:193. doi:10.3389/fimmu.2019.00193
37. Lin L, Kane N, Kobayashi N, et al. High-dose per fraction radiotherapy induces both antitumor immunity and immunosuppressive responses in prostate tumors. *Clin Cancer Res*. 2021;27(5):1505–1515. doi:10.1158/1078-0432.CCR-20-2293
38. Demaria S, Coleman CN, Formenti SC. Radiotherapy: changing the Game in Immunotherapy. *Trends Cancer*. 2016;2(6):286–294. doi:10.1016/j.trecan.2016.05.002
39. Huang RX, Zhou PK. DNA damage response signaling pathways and targets for radiotherapy sensitization in cancer. *Signal Transduct Targeted Ther*. 2020;5(1):60. doi:10.1038/s41392-020-0150-x
40. Loi S, Michiels S, Adams S, et al. The journey of tumor-infiltrating lymphocytes as a biomarker in breast cancer: clinical utility in an era of checkpoint inhibition. *Ann Oncol*. 2021;32(10):1236–1244. doi:10.1016/j.annonc.2021.07.007
41. Chen DS, Mellman I. Elements of cancer immunity and the cancer-immune set point. *Nature*. 2017;541(7637):321–330. doi:10.1038/nature21349
42. Fridman WH, Galon J, Pagès F, Tartour E, Sautès-Fridman C, Kroemer G. Prognostic and predictive impact of intra- and peritumoral immune infiltrates. *Cancer Res*. 2011;71(17):5601–5605. doi:10.1158/0008-5472.CAN-11-1316
43. Halama N, Michel S, Kloor M, et al. Localization and density of immune cells in the invasive margin of human colorectal cancer liver metastases are prognostic for response to chemotherapy. *Cancer Res*. 2011;71(17):5670–5677. doi:10.1158/0008-5472.CAN-11-0268
44. Haabeth OA, Tveita AA, Fauskanger M, et al. How Do CD4(+) T cells detect and eliminate tumor cells that either lack or express mhc class II molecules? *Front Immunol*. 2014;5:174. doi:10.3389/fimmu.2014.00174
45. Zander R, Schauder D, Xin G, et al. CD4(+) T cell help is required for the formation of a cytolytic CD8(+) T cell subset that protects against chronic infection and cancer. *Immunity*. 2019;51(6):1028–42.e4. doi:10.1016/j.immuni.2019.10.009
46. Aoki H, Ueha S, Shichino S, et al. TCR repertoire analysis reveals mobilization of novel CD8(+) T cell clones into the cancer-immunity cycle following anti-CD4 antibody administration. *Front Immunol*. 2018;9:3185. doi:10.3389/fimmu.2018.03185
47. Barsoumian HB, He K, Hsu E, et al. NLRP3 agonist enhances radiation-induced immune priming and promotes abscopal responses in anti-PD1 resistant model. *Cancer Immunol Immunother*. 2023;72(9):3003–3012. doi:10.1007/s00262-023-03471-x
48. Pang L, Guo S, Khan F, et al. Hypoxia-driven protease legumain promotes immunosuppression in glioblastoma. *Cell Rep Med*. 2023;4(11):101238. doi:10.1016/j.xcrm.2023.101238
49. Liu D, Hofman P. Expression of NOTCH1, NOTCH4, HLA-DMA and HLA-DRA is synergistically associated with T cell exclusion, immune checkpoint blockade efficacy and recurrence risk in ER-negative breast cancer. *Cell Oncol Dordr*. 2022;45(3):463–477. doi:10.1007/s13402-022-00677-6
50. Saito H, Ando S, Morishita N, et al. A combined lymphokine-activated killer (LAK) cell immunotherapy and adenovirus-p53 gene therapy for head and neck squamous cell carcinoma. *Anticancer Res*. 2014;34(7):3365–3370.
51. Textor S, Fiegler N, Arnold A, Porgador A, Hofmann TG, Cerwenka A. Human NK cells are alerted to induction of p53 in cancer cells by upregulation of the NKG2D ligands ULBP1 and ULBP2. *Cancer Res*. 2011;71(18):5998–6009. doi:10.1158/0008-5472.CAN-10-3211
52. Baumeister SH, Murad J, Werner L, et al. Phase I trial of autologous CAR T cells targeting NKG2D ligands in patients with AML/MDS and multiple myeloma. *Cancer Immunol Res*. 2019;7(1):100–112. doi:10.1158/2326-6066.CIR-18-0307